 CMC, vol.40, no.2, pp.145-163, 2014

Surface/interface Energy Effect on Electromechanical Responses Around a Nanosized Elliptical Inclusion under Far-field Loading at an Arbitrary Angle

Xue-Qian Fang[1,2], Hong-Wei Liu[1], Yong-Mao Zhao[1], Guo-Quan Nie[1] and Jin-Xi Liu[1]

Abstract: Electro-elastic surface/interface around nano-sized piezoelectric inclusions shows great effect on the response of piezoelectric nano-structures. In this paper, a theoretical model is proposed to examine the surface/interface effect on the electromechanical responses around a nano-sized elliptical piezoelectric inclusion embedded in an infinite piezoelectric matrix under far-field loading with an arbitrary angle, and the effect of loading angle is considered Combining the conformal mapping technique and electro-elastic surface/interface theory, a closed form solution of this problem is obtained and the interactive effect between the surface/interface and the aspect ratio of the elliptical inclusion is examined.

Keywords: Surface/interface energy electromechanical response elliptical inclusion, mapping method.

1 Introduction

Due to the excellent characters of miniaturization and harvesting the wasted energy such as sound vibration in the environment to produce electric power, piezoelectric nanostructures are attracting more and more interests in recent years In addition, they possess the outstanding nanosized piezoelectric and semiconducting properties. So, they are finding more and more applications for powering nano devices and sensors in the fields of medical science, defense technology, and environment/infrastructure monitoring. In the past decades, piezoelectric nanostructures have received considerable attention, and lots of theoretical [Nan and Wang (2013); Mohsen, Michael and Mitra (2013)] and experimental works [Kim et al. (2008); Beach et al. (2005)] have been done.

[1] Department of Engineering Mechanics, Shijiazhuang Tiedao University, Shijiazhuang, 050043, P. R. China.

[2] Corresponding author. Tel.: +86 311 87935514; Email: stduxfang@yeah.net

Compared with singlephase materials piezoelectric composites show higher sensitivity and lower mechanical losses. To enhance the serving behavior of piezoelectric composites, it is very requisite to investigate their responses on exterior loadings In engineering applications, piezoelectric materials are often used for transducers or actuators, and they will be subjected to combined mechanical and electrical loads. Characterizing the responses of piezoelectric nano-composites under an electromechanical load is fundamental for the optimum design of new piezoelectric nano-structures. To this end, lots of theoretical [Huang and Dai (2001); Iyer and Venkatesh (2014); Elata (2012)] and experimental [Jayendiran and Arockiarajan (2013); Li, Fang and Liu (2013)] investigations on the electromechanical response of piezoelectric composites have been dealt with. For anisotropic material as well as nonlinear problems, 'Computational Grains' method was proposed for the direct numerical simulation on the micromechanics of a large number of inclusions (for mechanical or electro-mechanical problems) without FEM meshing of inclusions/matrix [Dong and Atluri (2012); Dong and Atluri (2013); Bishay, Dong and Atluri (2014)]. When subjected to electrical and mechanical loads in service, the presence of inclusions and cracks can result in the premature failure. Since piezoelectric nano-composites made of ceramics are very popular in practical engineering, they are susceptible to a brittle fracture that can lead to a catastrophic failure. Hence, it is essential to precisely predict the behavior of defects embedded in piezoelectric nanocomposites under the influence of coupled electromechanical fields so that the integrity and reliability of piezoelectric components can be properly addressed.

For nano-sized piezoelectric composites, the electromechanical behavior is highly dependent on the interfacial properties between the nano-inclusion and the matrix due to the high surface-to-volume ratios When piezoelectric nano-structures are subjected to electrical and mechanical loads, the stress and electric displacement show significant variation with surface/interface. Therefore, it is important for us to understand the behavior resulting from the surface/interface around the nano-inclusions in piezoelectric nano-structures under the influence of coupled electromechanical fields. In recent year, the electro-elastic surface/interface model was proposed and widely used in predicting the behavior of nano-sized piezoelectric structures [Fang et al. (2013a); Nan and Wang (2013); Li, Chen, and Zeng (2013)].

To control the local elastic fields and minimize stress concentration caused by the surface/interface around an inclusion, the distribution of stress concentration under different loadings should be addressed. In the course of designing piezoelectric nanocomposites, elliptical nano-inclusions are often introduced to gain perfect performance of piezoelectric devices. A further optimization of the shape and interface of nano-inclusions can lead to a better overall performance of composites. The

interface effect of these elliptical inclusions on the electro-mechanical behavior, however, has rarely been addressed.

The purpose of the current paper is to provide a theoretical treatment for the nano-scale elliptical inclusion in piezoelectric materials under far-field loading at an arbitrary angle by combining the electro-elastic surface/interface model and complex variable method. To analyze the effect of interfacial properties on the stress and electric field within the nano-scale inclusion, the surface/interface theory in piezoelectric composites is introduced. Special attention is paid to the case of electromechanical loading at an arbitrary angle Numerical examples are given to illustrate the interactive effect of surface/interface and the aspect ratio of the elliptical inclusion on the stress and electric field

2 Problem formulation

An unbounded piezoelectric matrix with an elliptical piezoelectric inclusion of nano size is considered, as shown in Fig.1. The major and minor semi-axes of elliptical nano-inclusion are$a$ and b, respectively. It is assumed that both the nano-inclusion and matrix phases are transversely isotropic, with the symmetry along the z axis It is supposed that the piezoelectric matrix is subjected to far-field anti-plane shear loading τ_0 and in-plane electric field E_0 with an arbitrary angle β (see Fig. 1). The elastic stiffness, piezoelectric constant, dielectric constant, and mass density of elliptical nano-inclusion are denoted by c_{44}^I, e_{15}^I, χ_{11}^I and ρ^I. Those of the matrix are c_{44}^M, e_{15}^M, χ_{11}^M and ρ^M.

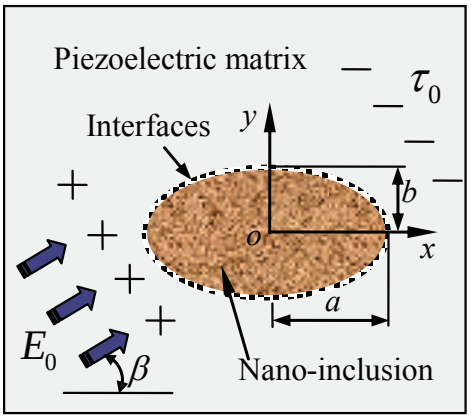

Figure 1: An elliptical nano-inclusion subjected to far-field loading at an arbitrary angle.

For the nano-size property, the surface/interface shows great effect on the strength and electric field around the nano-inclusion. According to the electro-elastic surface/interface theory in the previous literatures [Fang et al. (2013b); Li, Fang, and Liu (2013)], the interface region, which has its own electro-elastic properties, is regarded as a negligibly thin layer adhered to the nano-inclusion and matrix material. At the interface, the effect of interface stress and electric displacement should be considered. The material properties of interface are different from the matrix and nano-inclusion, and denoted by c_{44}^S, e_{15}^S, χ_{11}^S and ρ^S.

Due to the character of far-field loading, only the out-of-plane displacement w and the in-plane electric fields φ need to be considered. In the following, the generalized displacements $\mathbf{f}$, the generalized strains $\mathbf{F}_j$, and the generalized stresses $\mathbf{\Theta}_j$ are introduced, i.e.,

$$\mathbf{f} = [\mathbf{w}, \varphi]^{\mathbf{T}}, \tag{1}$$

$$\mathbf{F}_j = [\gamma_{jz}, E_j]^T, \quad (j = r, \theta \text{ or } j = x, y), \tag{2}$$

$$\mathbf{\Theta}_j = [\tau_{jz}, D_j]^T, \quad (j = r, \theta \text{ or } j = x, y). \tag{3}$$

where γ_{jz} and E_j are the components of shear strain and electric field, respectively. τ_{jz} and D_j denote the components of shear stress and electric displacement, respectively.

The governing equations for piezoelectric materials under far field anti-plane loading and in-plane electrical field can be expressed as

$$\nabla^2 \mathbf{f} = 0, \tag{4}$$

$$\mathbf{\Theta}_r - \mathrm{i}\mathbf{\Theta}_\theta = \mathbf{L}\left(\mathbf{F}_r - \mathrm{i}\mathbf{F}_\theta\right) = \mathbf{L}\left(\frac{\partial \mathbf{f}}{\partial r} - i\frac{\partial \mathbf{f}}{r\partial \theta}\right), \tag{5}$$

where $\mathbf{L} = \begin{bmatrix} c_{44} & e_{15} \\ e_{15} & -\chi_{11} \end{bmatrix}$.

3 Mapping method for the elliptical nano-inclusion

To apply the non-classical boundary conditions, the conformal mapping method is introduced. Then, the problem of elliptical nano-inclusions in the $z = x + \mathrm{i}y$ plane can be transformed into the problem of circular nano-inclusions in the $\zeta = \xi + \mathrm{i}\eta$ plane, as shown in Fig. 2. The transform function is expressed as

$$z = g(\zeta) = \frac{c}{2}\left(R\zeta + \frac{1}{R\zeta}\right), \quad \zeta(\bar{r}, \theta) = \bar{r}e^{\mathrm{i}\theta}, \tag{6}$$

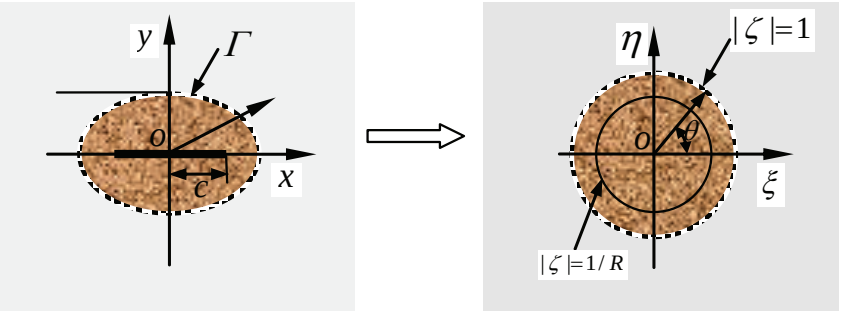

Figure 2: Mapping method of elliptical nano-inclusion with electro-elastic surface/interface effect.

where $c=\sqrt{a^2-b^2}$and $R=\sqrt{(a+b)/(a-b)}$. This transformation can map the exterior of the elliptical nano-inclusion in the z-plane into the exterior of the unit circle in the ζ-plane, and interior into the annulus region between $1/R<\bar{r}<1$. The circle of $\bar{r}=1/R$ represents a cut from -c to +c on the z-plane.

The solution of Laplace equation (4) can be obtained by letting $\mathbf{f}$ be the real part of some analytic functions such that

$$\mathbf{f}=\mathrm{Re}\mathbf{U}(z)=\mathrm{Re}\mathbf{U}[g(\zeta)], \tag{7}$$

where Re denotes the real part.

The generalized strains and stresses can be written as

$$\mathbf{F}_r-i\mathbf{F}_\theta=e^{i\theta}\mathbf{U}', \tag{8}$$

$$\mathbf{\Theta}_r-\mathrm{i}\mathbf{\Theta}_\theta=e^{i\theta}\mathbf{L}\frac{d\mathbf{U}(z)}{dz}. \tag{9}$$

4 Field solutions around the elliptical nano-inclusion under the generalized loading

To obtain the closed form solutions of the loadings with an arbitrary angle, the angle is generalized by superposing two different far-field loadings [Mishra et al. (2013)]. The first kind of loading is a horizontal far-field loading ($\beta=0$), and the second kind is a vertical far-field loading ($\beta=\frac{\pi}{2}$). Then, the terms of $\cos\beta$ and $\sin\beta$ in the expressions of displacement and electric field are superposed to obtain a generalized solution in terms of far-field loading angle β.

In the ζ-plane, the polynomial solutions for the piezoelectric matrix and the nano-inclusion under horizontal loading are expressed as

$$\mathbf{U}_h^M = -\left[\left\{\begin{array}{c} A_1 \\ A_3 \end{array}\right\}\zeta - \left\{\begin{array}{c} A_2 \\ A_4 \end{array}\right\}\frac{1}{\zeta}\right], \tag{10}$$

$$\mathbf{U}_h^I = -\left[\left\{\begin{array}{c} B_1 \\ B_3 \end{array}\right\}\zeta - \left\{\begin{array}{c} B_2 \\ B_4 \end{array}\right\}\frac{1}{\zeta}\right]. \tag{11}$$

The polynomial solutions under vertical loading are expressed as

$$\mathbf{U}_v^M = -\mathrm{i}\left[\left\{\begin{array}{c} \bar{A}_1 \\ \bar{A}_3 \end{array}\right\}\zeta - \left\{\begin{array}{c} \bar{A}_2 \\ \bar{A}_4 \end{array}\right\}\frac{1}{\zeta}\right], \tag{12}$$

$$\mathbf{U}_v^I = -\mathrm{i}\left[\left\{\begin{array}{c} \bar{B}_1 \\ \bar{B}_3 \end{array}\right\}\zeta - \left\{\begin{array}{c} \bar{B}_2 \\ \bar{B}_4 \end{array}\right\}\frac{1}{\zeta}\right]. \tag{13}$$

It is noted that $A_j, \bar{A}_j, B_j$ and $\bar{B}_j (j = 1-4)$ are the real constant to be determined by satisfying the boundary conditions of far-field and surface/interface. The relations between A_j, B_j and $\bar{A}_j, \bar{B}_j$ are $\bar{A}_j = -A_j$ and $\bar{B}_j = -B_j$.

The closed form solutions in the regions of matrix and nano-inclusion are expressed as

In the matrix,

$$\mathbf{U}_z^M = \left[\left\{\begin{array}{c} A_1 \\ A_3 \end{array}\right\}\bar{r} + \left\{\begin{array}{c} A_2 \\ A_4 \end{array}\right\}\frac{1}{\bar{r}}\right]\cos(\theta-\beta), \tag{14}$$

$$\mathbf{F}_{\bar{r}}^M = \frac{2}{cRh}\left[\left\{\begin{array}{c} A_1 \\ -A_3 \end{array}\right\}\bar{r}^2 + \left\{\begin{array}{c} -A_2 \\ A_4 \end{array}\right\}\right]\cos(\theta-\beta), \tag{15}$$

$$\mathbf{F}_{\theta}^M = \frac{2}{cRh}\left[\left\{\begin{array}{c} -A_1 \\ A_3 \end{array}\right\}\bar{r}^2 + \left\{\begin{array}{c} -A_2 \\ A_4 \end{array}\right\}\right]\sin(\theta-\beta), \tag{16}$$

$$\mathbf{\Theta}_{\bar{r}}^M = \frac{2}{cRh}\left[\left\{\begin{array}{c} c_{44}^M \\ e_{15}^M \end{array}\right\}(A_1\bar{r}^2 - A_2) + \left\{\begin{array}{c} e_{15}^M \\ -\varepsilon_{11}^M \end{array}\right\}(A_3\bar{r}^2 - A_4)\right]\cos(\theta-\beta), \tag{17}$$

$$\mathbf{\Theta}_{\theta}^M = -\frac{2}{cRh}\left[\left\{\begin{array}{c} c_{44}^M \\ e_{15}^M \end{array}\right\}(A_1\bar{r}^2 + A_2) + \left\{\begin{array}{c} e_{15}^M \\ -\chi_{11}^M \end{array}\right\}(A_3\bar{r}^2 + A_4)\right]\sin(\theta-\beta). \tag{18}$$

Inside the nano-inclusion,

$$\mathbf{U}_z^I = \left[\left\{\begin{array}{c} B_1 \\ B_3 \end{array}\right\}\bar{r} + \left\{\begin{array}{c} B_2 \\ B_4 \end{array}\right\}\frac{1}{\bar{r}}\right]\cos(\theta-\beta), \tag{19}$$

$$\mathbf{F}_{\bar{r}}^{I}=\frac{2}{cRh}\left[\left\{\begin{array}{c}B_1\\-B_3\end{array}\right\}\bar{r}^2+\left\{\begin{array}{c}-B_2\\B_4\end{array}\right\}\right]\cos(\theta-\beta), \tag{20}$$

$$\mathbf{F}_{\theta}^{I}=\frac{2}{cRh}\left[\left\{\begin{array}{c}-B_1\\B_3\end{array}\right\}\bar{r}^2+\left\{\begin{array}{c}-B_2\\B_4\end{array}\right\}\right]\sin(\theta-\beta), \tag{21}$$

$$\mathbf{\Theta}_{\bar{r}}^{I}=\frac{2}{cRh}\left[\left\{\begin{array}{c}c_{44}^{I}\\e_{15}^{I}\end{array}\right\}(B_1\bar{r}^2-B_2)+\left\{\begin{array}{c}e_{15}^{I}\\-\chi_{11}^{I}\end{array}\right\}(B_3\bar{r}^2-B_4)\right]\cos(\theta-\beta), \tag{22}$$

$$\mathbf{\Theta}_{\theta}^{I}=-\frac{2}{cRh}\left[\left\{\begin{array}{c}c_{44}^{I}\\e_{15}^{I}\end{array}\right\}(B_1\bar{r}^2+B_2)+\left\{\begin{array}{c}e_{15}^{I}\\-\chi_{11}^{I}\end{array}\right\}(B_3\bar{r}^2+B_4)\right]\sin(\theta-\beta), \tag{23}$$

where $h=\sqrt{\bar{r}^4-cR\bar{r}^2\cos 2\theta+(1/R^4)}$.

The far field conditions for both loading cases can be expressed as

$$\tau_{rz}^{M}|_{\bar{r}\to\infty}=\tau_{\theta z}^{M}|_{\bar{r}\to\infty}=\tau_0, \tag{24}$$

$$E_{r}^{M}|_{\bar{r}\to\infty}=E_{\theta}^{M}|_{\bar{r}\to\infty}=E_0. \tag{25}$$

Two additional equations can be obtained by letting

$$\mathbf{f}_{z}^{I}(e^{i\theta}/R)=\mathbf{f}_{z}^{I}(e^{-i\theta}/R). \tag{26}$$

With consideration of interface effects, the boundary conditions along the elliptical nano-inclusion under the far-field loading at an arbitrary angle can be described by

$$\mathbf{f}^{M}|_{\bar{r}=1}=\mathbf{f}^{I}|_{\bar{r}=1}, \tag{27}$$

$$\mathbf{\Theta}_{\bar{r}}^{M}|_{\bar{r}=1}-\mathbf{\Theta}_{\bar{r}}^{I}|_{\bar{r}=1}=\frac{1}{\bar{r}}\frac{\partial\mathbf{\Theta}_{\theta}^{S}}{\partial\theta}|_{\bar{r}=1}, \tag{28}$$

where the surface stress tensor and electric displacement can be expressed as

$$\mathbf{\Theta}_{\theta}^{S}=\mathbf{L}^{S}\mathbf{F}_{\theta}^{S}, \tag{29}$$

Here $\mathbf{L}^{S}=\left[\begin{array}{cc}c_{44}^{S} & e_{15}^{S}\\ e_{15}^{S} & -\varepsilon_{11}^{S}\end{array}\right]$ are the material properties of surface/interface, which can be calculated from atomistic simulations.

In this study, a coherent interface is considered. At the boundary, the interfacial strain and electric potential are equal to the associated tangential strain and electric potential in the abutting bulk materials, respectively. They can be expressed as

$$\mathbf{F}_{\theta}^{S}(\Gamma)=\mathbf{F}_{\theta}^{I}(\Gamma)=\mathbf{F}_{\theta}^{C}(\Gamma). \tag{30}$$

Substituting Eqs. (14)-(23) into Eqs. (24)-(28), the expressions of A_i and $B_i(i=1-4)$ which are shown in Appendix can be obtained.

5 Numerical examples and analysis

For piezoelectric nanocomposites with nano-inclusion under static or dynamic loading, the distribution of stress near the interface is primarily responsible for the stiffness reduction, and the electric field is important for producing high electric potential.

In the following, the material properties of matrix are $c_{44}^M = 3.53 \times 10^{10} N/m^2$, $e_{15}^M = 17 C/m^2$, $\chi_{11}^M = 1.51 \times 10^{-8} C^2/Nm^2$, the far-field mechanical loading is $\sigma_0 = 100 MPa$, and the far-field electrical loading is $E_0 = 10^6 V/m$.

5.1 Stress distribution

The stress distribution pattern under different electro-elastic properties of surface/interface around the nano-inclusion is illustrated. This can provide us information on the points of stress concentrations and therefore the possible locations of failure and fracture.

Fig. 3 shows the stress distribution along the x axis. It can be seen that the stress inverts its sign due to the existence of surface/interface. At the boundary, the surface/interface effect on the stress in the matrix is greater than that inside the nano-inclusion. At the center, the effect is the maximum. It is noted that the numerical results without surface/interface effect are consistent with those of Mishra et al. (2013).

To illustrate the surface/interface effect on the stress in the case of soft nano-inclusion, Fig. 4 is presented. It can be seen that the surface/interface shows greater effect on the stress in the matrix than that inside the nano-inclusion. The absolute value of stress decreases with the values of material properties of surface/interface. At the boundary, the stress inside the nano-inclusion is smaller than that in the matrix. The jump of stress at the boundary becomes significant if the values of material properties of surface/interface decrease. When the surface/interface is stiffer than the nano-inclusion and matrix, the stress decreases greatly and the jump of stress becomes small.

In Fig. 5, the nano-inclusion is stiffer than the matrix. At the boundary, the stress in the nano-inclusion is greater than that in the matrix. By comparing with the results in Fig. 4, it is clear that the interface effect decreases due to the stiff nano-inclusion. The jump of stress at the boundary also decreases. The surface/interface effect on the stress inside the nano-inclusion is greater than that in the matrix. Therefore, a stiff inclusion is proposed to reduce the jump of stress at the boundary because of surface/interface effect.

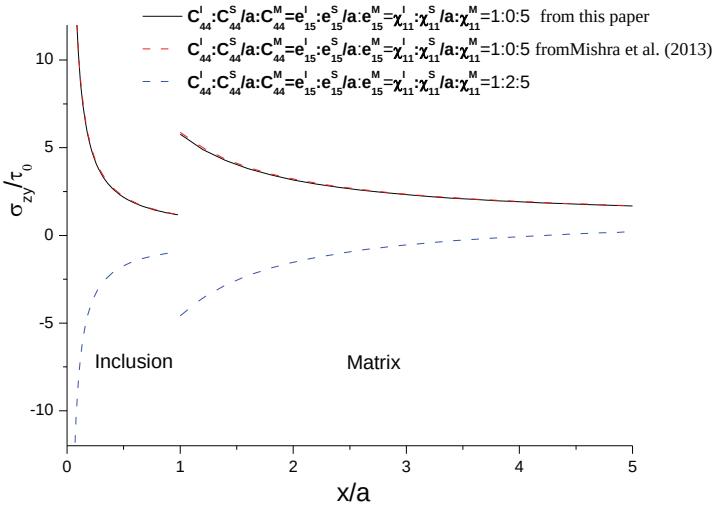

Figure 3: Comparison of stress distribution along the $x$axis with results obtained from Mishra et al. (2013) in the case of soft nano-inclusion ($b/a = 1/5$, $\beta = \pi/2$).

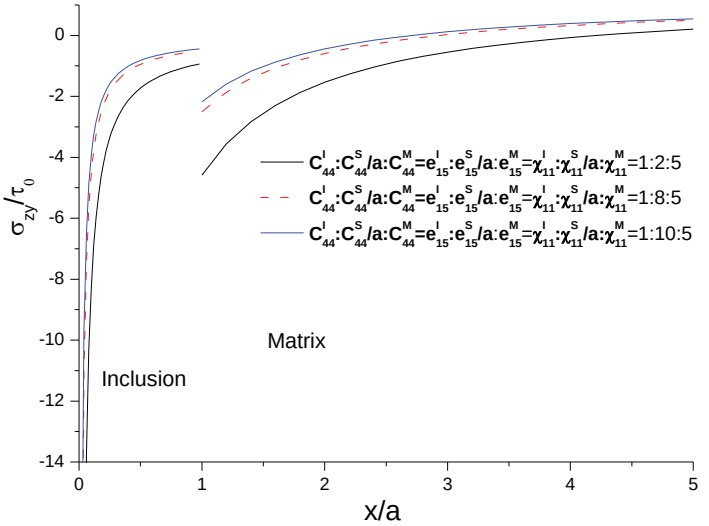

Figure 4: Stress distribution along the $x$axis with different interfaces in the case of soft nano-inclusion ($b/a = 1/5$, $\beta = \pi/2$).

5.2 Electric field distribution

For piezoelectric composites, the producing electric power is an important character. From the perspective of engineering applications for piezoelectric devices, it is

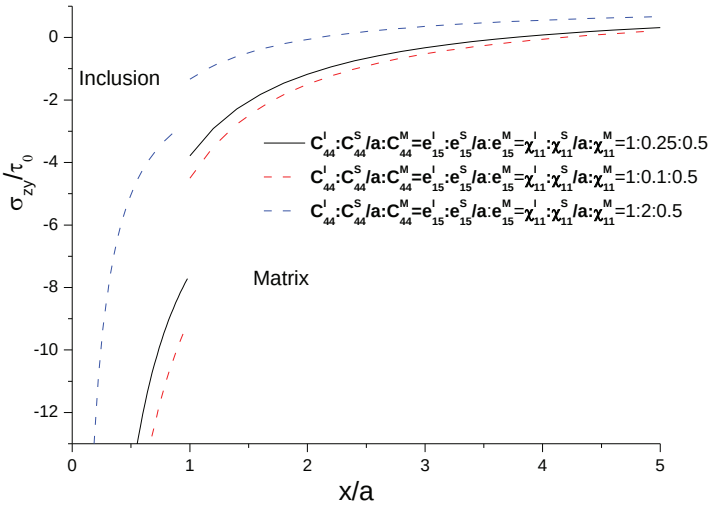

Figure 5: Stress distribution along the x axis in the case of stiff nano-inclusion ($b/a = 1/5$, $\beta = \pi/2$).

very necessary to understand the nature of electric field distribution.

Fig. 6 shows the electric field distribution along the x axis. It can be seen that the electric field increases significantly due to the existence of surface/interface around the elliptical nano-inclusion. At the boundary, the surface/interface effect is the maximum. By comparing with the results in Fig. 3, it is clear that the interface effect on the stress is greater than that on the electric field. In Fig. 7, the electric field distribution with different piezoelectric properties of surface/interface is presented. The electric field concentration decreases significantly with increasing the piezoelectric properties of surface/interface, especially at the boundary of nano-inclusion.

Fig. 8 shows the electric field distribution along the x axis in the case of nano-inclusion with poor electric property. By comparing with the results in Fig. 7, it can be seen that the surface/interface effect decreases if the nano-inclusion possesses poor electric property.

5.3 Effect of loading angle under different surfaces/interfaces

To find the effect of loading angle under different properties of surface/interface, Figs. 9-10 are given. In Fig. 9, the loading angle is $\beta = 0$. By comparing with the results in Fig. 5, it can be seen that the stress field along the x axis inverts its sign due to the variation of loading angle. In Fig. 10, the loading angle is $\beta = \pi/4$.

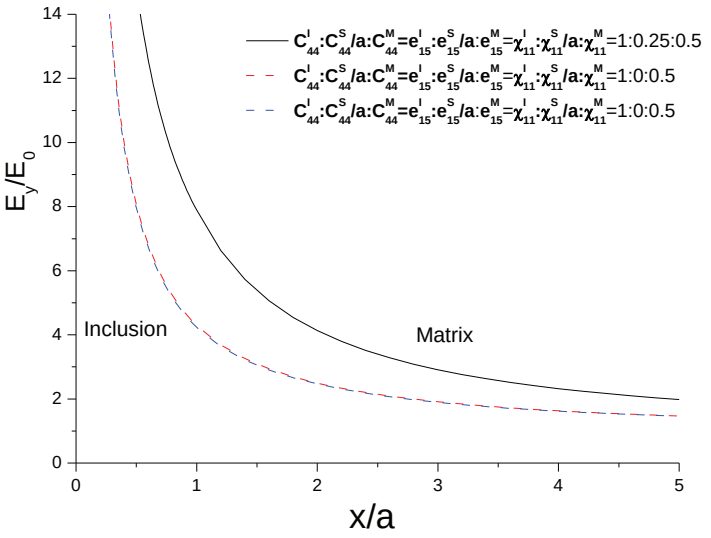

Figure 6: Comparison of electric field distribution along the x axis with results obtained from Mishra et al. (2013) in the case of nano-inclusion with strong piezoelectric property ($b/a = 1/5$, $\beta = \pi/2$).

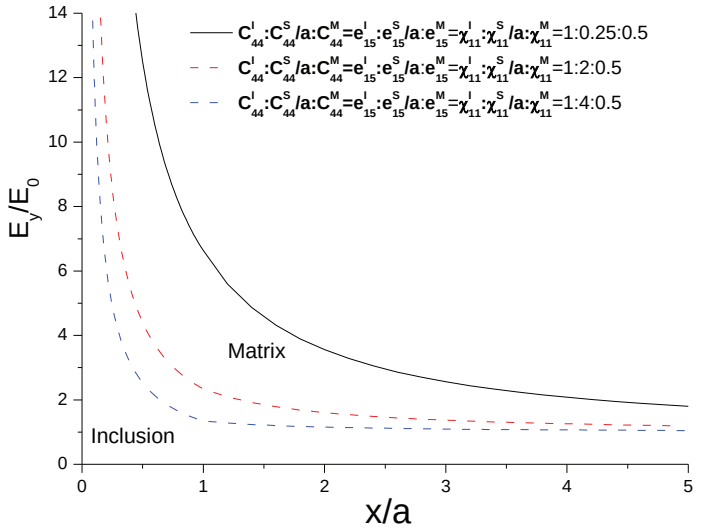

Figure 7: Electric field distribution along the x axis in the case of nano-inclusion with strong piezoelectric property ($b/a = 1/5$, $\beta = \pi/2$).

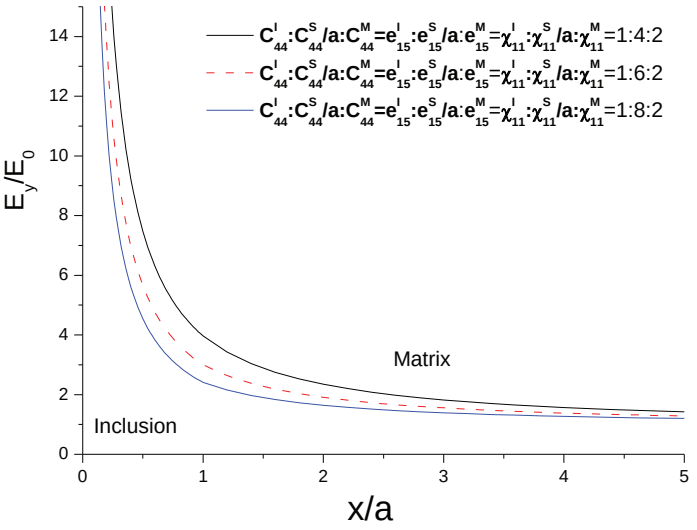

Figure 8: Electric field distribution along the x axis in the case of nano-inclusion with poor piezoelectric property ($b/a = 1/5$, $\beta = \pi/2$).

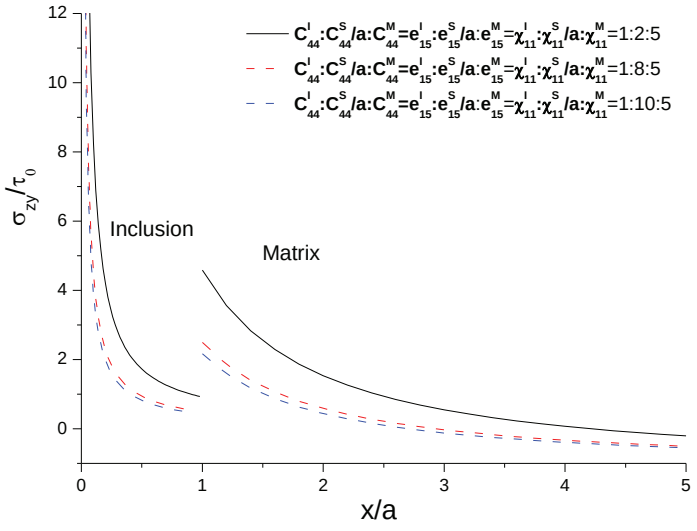

Figure 9: Stress distribution along the x axis in the case of stiff nano-inclusion ($b/a = 1/5$, $\beta = 0$).

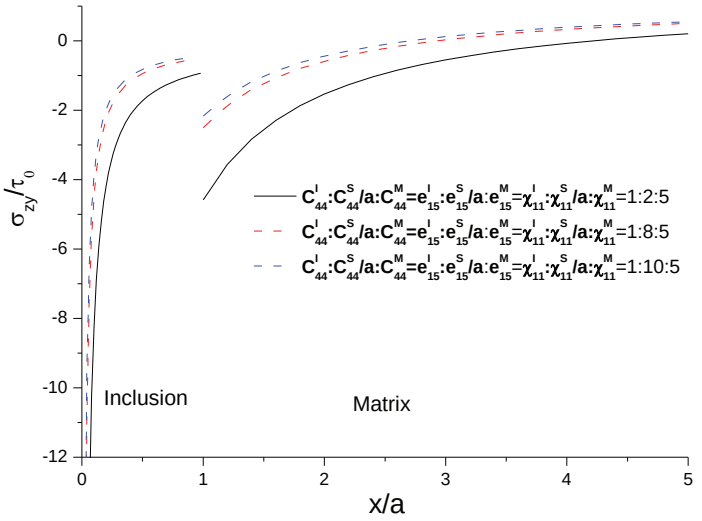

Figure 10: Stress distribution along the x axis in the case of stiff nano-inclusion ($b/a = 1/5$, $\beta = \pi/4$).

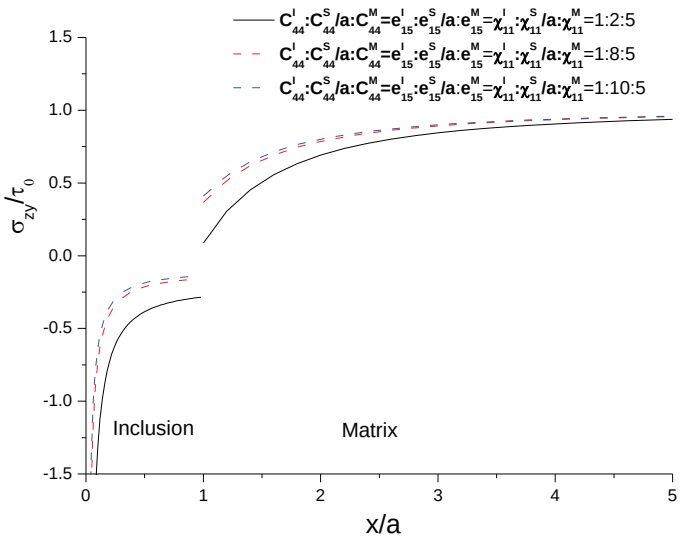

Figure 11: Stress distribution along the $x$axis in the case of stiff nano-inclusion ($b/a = 1/2$, $\beta = \pi/2$).

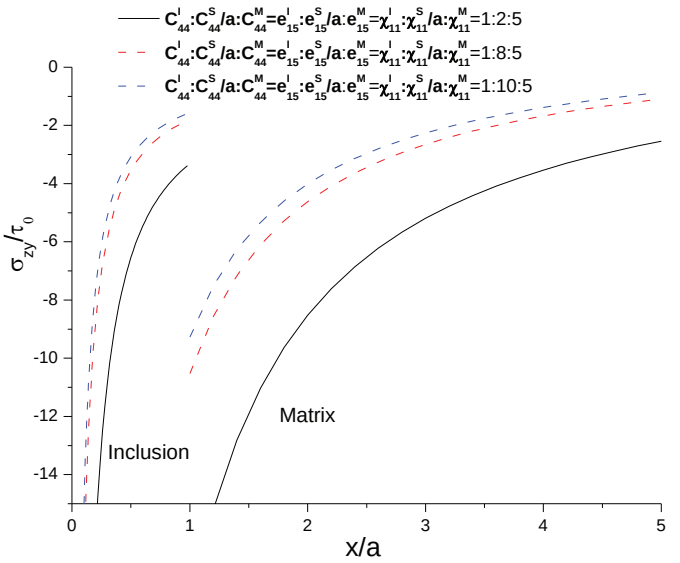

Figure 12: Stress distribution along the $x$axis in the case of stiff nano-inclusion ($b/a = 1/10$, $\beta = \pi/2$).

It can be seen that the surface/interface effect increases significantly due to the variation of loading angle. The jump of stress at the boundary becomes smaller when the values of material properties of surface/interface increase.

5.4 Effect of shape of elliptical nano-inclusion under different surfaces/interfaces

To find the shape effect of elliptical nano-inclusion on the stress distribution under different surfaces/interfaces, Figs. 11 and 12 are presented. The value of b/a in Fig. 11 is greater than that in Fig. 12. It is clear that the stress shows a significant increase if the value of b/a becomes smaller. The surface/interface effect also increases significantly because of a smaller value of b/a.

6 Conclusion

An analytical model has been developed to evaluate the electro-mechanical response of piezoelectric nanocomposites with elliptical nano-inclusion under far-field loading at an arbitrary angle. The explicit closedform solutions of stress and electric fields are presented, and some significant findings are found.

a. The shape of the elliptical nano-inclusion shows significant effect on the stress and electric field. The surface/interface effect increases greatly if the value of b/a

becomes smaller.

b. Due to the existence of surface/interface, the stress and electric field around the nano-inclusion show significant variation. The surface/interface shows greater effect on the stress than that on the electric field.

c. If the nano-inclusion is stiff, the surface/interface effect on the stress inside the nano-inclusion becomes significant; however, the jump of stress at the boundary is small.

d. The surface/interface effect decreases if the nano-inclusion possesses poor electric property.

Acknowledgement: The paper is supported by Key Project of Hebei Education Department of China (ZD2014035), National Natural Science Foundation of China (Nos. 11172185; 11272222), Natural Science Foundation for Outstanding Young Researcher in Hebei Province of China (No. A2014210015), and National Natural Science Foundation in Hebei Province of China (A2013210106).

References

Beach, G. S. D.; Nistor, C.; Knutson, C.; Tsoi, M.; Erskine, J. L. (2005): Dynamics of field-driven domain-wall propagation in ferromagnetic nanowires. *Nature Materials*, vol. 4, pp. 741–744.

Bishay, P. L.; Dong, L.; Atluri, S. N. (2014): Multi-physics computational grains (MPCGs) for direct numerical simulation (DNS) of piezoelectric composite/porous materials and structures. *Computational Mechanics*, DOI: 10.1007/s00466-014-1044-y.

Dong, L.; Atluri, S. N. (2012): Development of 3D trefftz voronoi cells with ellipsoidal voids &/or elastic/rigid inclusions for micromechanical modeling of heterogeneous materials. *CMC: Computers, Materials & Continua*, vol. 30, no. 1, pp. 39– 81.

Dong, L.; Atluri, S. N. (2013): SGBEM Voronoi Cells (SVCs), with embedded arbitrary shaped inclusions, voids, and/or cracks, for micromechanical modeling of heterogeneous materials. *CMC: Computers, Materials & Continua*, vol. 33, no. 2, pp.111–154.

Elata, D. (2012): The electromechanical response of a symmetric electret parallel-plates actuator. *Sensors and Actuators A*, vol. 173, pp.197–201.

Fang, X. Q.; Liu, X. L.; Huang, M. J.; Liu, J. X. (2013a): Dynamic effective shear modulus of nanocomposites containing randomly distributed elliptical nanofibers with interface effect. *Composites Science and Technology*, vol. 87, pp.64–68.

Fang, X. Q.; Liu, X. L.; Liu, J. X.; Nie, G. Q. (2013b): Anti-plane electromechanical behavior of piezoelectric composites with a piezoelectric nano-fiber. *Journal of Applied Physics*, vol. 114, pp.054310.

Huang, J. H.; Dai, W. L. (2001): Static and dynamic electromechanical responses of piezoelectric transducers. *Materials Letters*, vol. 50, pp.209–218.

Iyer, S.; Venkatesh, T. A. (2014): Electromechanical response of (3-0, 3-1) particulate, fibrous, and porous piezoelectric composites with anisotropic constituents: A model based on the homogenization method. *International Journal of Solids and Structures*, vol. 51, pp.1221–1234.

Jayendiran, R.; Arockiarajan, A. (2013): Non-linear electromechanical response of 1-3 type piezocomposites. *International Journal of Solids and Structures*, vol. 50, pp.2259–2270.

Kim, J.; Yang, S. A.; Choi, Y. C.; Han, J. K.; Jeong, K. O.; Yun, Y. J.; Kim, D. J.; Yang, S. M.; Yoon, D.; Cheong, H.; Chang, K. S.; Noh, T. W.; Bu, S. D. (2008): Ferroelectricity in highly ordered arrays of ultra-thin-walled Pb(Zr,Ti)O3 nanotubes composed of nanometer-sized perovskite crystallites. *Nano Letters*, vol. 8 , pp.1813–1818.

Li, J.; Fang, Q. H.; Liu, Y. W. (2013): Crack interaction with a second phase nanoscale circular inclusion in an elastic matrix. *International Journal of Engineering Science*, vol. 72, pp.89–97.

Li, T.; Chen, L.; Zeng, K. Y. (2013): In situ studies of nanoscale electromechanical behavior of nacre under flexural stresses using band excitation PFM. *Acta Biomaterialia*, vol. 9, pp.5903–5912.

Mishra, D.; Park, C. Y.; Yoo, S. H.; Pak, Y. E. (2013): Closed-form solution for elliptical inclusion problem in antiplane piezoelectricity with far-field loading at an arbitrary angle. *European Journal of Mechanics A/Solids*, vol. 40, pp.186–197.

Mohsen, P.; Michael, A. S.; Mitra, D. (2013): A theoretical study on the effect of piezoelectric charges on the surface potential and surface depletion region of ZnO nanowires. *Semiconductor Science and Technology*, vol. 28, pp.15–19.

Nan, H. S.; Wang, B. L. (2013): Effect of crack face residual surface stress on nanoscale fracture of piezoelectric materials. *Engineering Fracture Mechanics*, vol. 110, pp.68–80.

Appendix A

$$A_1 = p(e_{15}^M E_0 + \tau_0)/c_{44}^M, \tag{A1}$$

$$
\begin{aligned}
A_2 = p((&-\tau_0 c_{44}^I + \tau_0 c_{44}^S + \tau_0 c_{44}^M)\varepsilon_{11}^I - \tau_0 (e_{15}^I)^2 \\
&+(2E_0 c_{44}^M e_{15}^I + \tau_0 c_{44}^S - \tau_0 c_{44}^I + \tau_0 c_{44}^M)\varepsilon_{11}^M \\
&+(-\tau_0 c_{44}^I + \tau_0 c_{44}^S + \tau_0 c_{44}^M)\varepsilon_{11}^S + (2E_0 c_{44}^M \varepsilon_{11}^M + \tau_0 e_{15}^S)e_{15}^S \\
&+((-E_0 c_{44}^M - E_0 c_{44}^I + E_0 c_{44}^S)\varepsilon_{11}^I - E_0 (e_{15}^I)^2 \\
&+(E_0 c_{44}^S - E_0 c_{44}^I + E_0 c_{44}^M)\varepsilon_{11}^M + (-E_0 c_{44}^M - E_0 c_{44}^I + E_0 c_{44}^S)\varepsilon_{11}^S \\
&+(2\tau_0 + E_0 e_{15}^S)e_{15}^S + (\tau_0 + 2E_0 e_{15}^S + E_0 e_{15}^M)e_{15}^M \\
&+(2\tau_0 c_{44}^I \varepsilon_{11}^I + 2\tau_0 (e_{15}^I)^2 + (2\tau_0 c_{44}^M + 2\tau_0 c_{44}^S)\varepsilon_{11}^M + (2\tau_0 c_{44}^M + 2\tau_0 c_{44}^S)\varepsilon_{11}^S \\
&+(4E_0 c_{44}^M \varepsilon_{11}^M + 2\tau_0 e_{15}^S)e_{15}^S + (2E_0 c_{44}^I \varepsilon_{11}^I + 2E_0 (e_{15}^I)^2 \\
&+(2E_0 c_{44}^M + 2E_0 c_{44}^S)\varepsilon_{11}^M + (-2E_0 c_{44}^M + 2E_0 c_{44}^S)\varepsilon_{11}^S \\
&+(4\tau_0 + 2E_0 e_{15}^S)e_{15}^S + (4E_0 e_{15}^S + 2\tau_0 + 2e_{15}^M E_0)e_{15}^M \\
&+((-\tau_0 c_{44}^S - \tau_0 c_{44}^M - \tau_0 c_{44}^I)\varepsilon_{11}^I - \tau_0 (e_{15}^I)^2 + (-2E_0 c_{44}^M e_{15}^I \\
&+\tau_0 c_{44}^S + \tau_0 c_{44}^I + \tau_0 c_{44}^M)\varepsilon_{11}^M + (\tau_0 c_{44}^I + \tau_0 c_{44}^S + \tau_0 c_{44}^M)\varepsilon_{11}^S \\
&+(2E_0 c_{44}^M \varepsilon_{11}^M + \tau_0 e_{15}^S)e_{15}^S + ((-E_0 c_{44}^I + E_0 c_{44}^M - E_0 c_{44}^S)\varepsilon_{11}^I \\
&-E_0 (e_{15}^I)^2 + (E_0 c_{44}^S + E_0 c_{44}^I + E_0 c_{44}^M)\varepsilon_{11}^M \\
&+(-E_0 c_{44}^M + E_0 c_{44}^I + E_0 c_{44}^S)\varepsilon_{11}^S + (2\tau_0 + E_0 e_{15}^S)e_{15}^S \\
&+(\tau_0 + 2E_0 e_{15}^S + e_{15}^M E_0)e_{15}^M)q)q)/c_{44}^M/((c_{44}^I + c_{44}^M - c_{44}^S)\varepsilon_{11}^I \\
&+(e_{15}^I)^2 + (c_{44}^I + c_{44}^M - c_{44}^S)\varepsilon_{11}^M + (c_{44}^I + c_{44}^M - c_{44}^S)\varepsilon_{11}^S - e_{15}^S \\
&+(2e_{15}^I + e_{15}^M)e_{15}^M + (-2(e_{15}^I)^2 - 2c_{44}^I \varepsilon_{11}^I + (-2c_{44}^S + 2c_{44}^M)\varepsilon_{11}^M \\
&+(-2c_{44}^S + 2c_{44}^M) \times \varepsilon_{11}^S - 2(e_{15}^S)^2 + 2(e_{15}^M)^2 + ((c_{44}^I - c_{44}^M + c_{44}^S)\varepsilon_{11}^I \\
&+(e_{15}^I)^2 + (-c_{44}^I + c_{44}^M - c_{44}^S)\varepsilon_{11}^M + (-c_{44}^I + c_{44}^M - c_{44}^S) \\
&\times \varepsilon_{11}^S - (e_{15}^S)^2 + (-2e_{15}^I + e_{15}^M)e_{15}^M)q)q),
\end{aligned}
\tag{A2}
$$

$$
A_3 = -pE_0, \tag{A3}
$$

$$
\begin{aligned}
A_4 = -p(&\left(-E_0 c_{44}^M + E_0 c_{44}^S - E_0 c_{44}^I\right) c_{44}^M \varepsilon_{11}^I + \left(-2\tau_0 c_{44}^M - E_0 c_{44}^M e_{15}^I\right) e_{15}^I \\
&+\left(E_0 c_{44}^I - E_0 c_{44}^S + E_0 c_{44}^M\right) \times c_{44}^M \varepsilon_{11}^M + (-E_0 c_{44}^M + E_0 c_{44}^S - E_0 c_{44}^I) c_{44}^M \varepsilon_{11}^S \\
&+(2\tau_0 c_{44}^M + E_0 c_{44}^M e_{15}^S)e_{15}^S + (2\tau_0 c_{44}^I - 2E_0 c_{44}^M e_{15}^I - 2\tau_0 c_{44}^S \\
&+(2E_0 c_{44}^I - 2E_0 c_{44}^S + E_0 c_{44}^M)e_{15}^M)e_{15}^M + (2E_0 c_{44}^M c_{44}^I \varepsilon_{11}^I + 2E_0 c_{44}^M (e_{15}^I)^2 \\
&+(-2E_0 c_{44}^S + 2E_0 c_{44}^M) \times c_{44}^M \varepsilon_{11}^M + \left(2E_0 c_{44}^S - 2E_0 c_{44}^M\right) c_{44}^M \varepsilon_{11}^S \\
&+\left(4\tau_0 c_{44}^M + 2E_0 c_{44}^M e_{15}^S\right) e_{15}^S + (-4\tau_0 c_{44}^S + (-4E_0 c_{44}^S + 2E_0 c_{44}^M) \times e_{15}^M)e_{15}^M \\
&+\left(\left(-E_0 c_{44}^I + E_0 c_{44}^M - E_0 c_{44}^S\right) c_{44}^M \varepsilon_{11}^I + \left(2\tau_0 c_{44}^M - E_0 c_{44}^M e_{15}^I\right) e_{15}^I \right. \\
&\left.+\left(-E_0 c_{44}^I + E_0 c_{44}^M - E_0 c_{44}^S\right) \times c_{44}^M \varepsilon_{11}^M + (-E_0 c_{44}^M + E_0 c_{44}^S + E_0 c_{44}^I) c_{44}^M \varepsilon_{11}^S \right. \\
&+(2\tau_0 c_{44}^M + E_0 c_{44}^M e_{15}^S)e_{15}^S + (-2\tau_0 c_{44}^I - 2\tau_0 c_{44}^S + 2E_0 c_{44}^M e_{15}^I \\
&+(-2E_0 c_{44}^I + E_0 c_{44}^M - 2E_0 c_{44}^S)e_{15}^M)e_{15}^M)q)q)/c_{44}^M/((c_{44}^M - c_{44}^S + c_{44}^I)\varepsilon_{11}^I \\
&+(e_{15}^I)^2 + (c_{44}^M - c_{44}^S + c_{44}^I)\varepsilon_{11}^M + (c_{44}^M - c_{44}^S + c_{44}^I)\varepsilon_{11}^S - (e_{15}^S)^2 \\
&+(2e_{15}^I + e_{15}^M)e_{15}^M + (-2(e_{15}^I)^2 - 2c_{44}^I \varepsilon_{11}^I + (2c_{44}^M - 2c_{44}^S)\varepsilon_{11}^M + (2c_{44}^M - 2c_{44}^S) \\
&\times \varepsilon_{11}^S - 2(e_{15}^S)^2 + 2(e_{15}^M)^2 + ((-c_{44}^M + c_{44}^I + c_{44}^S)\varepsilon_{11}^I + (e_{15}^I)^2 + (c_{44}^M - c_{44}^S - c_{44}^I)\varepsilon_{11}^M \\
&+(c_{44}^M - c_{44}^S - c_{44}^I)\varepsilon_{11}^S - (e_{15}^S)^2 + (-2e_{15}^I + e_{15}^M)e_{15}^M)q)q),
\end{aligned}
\tag{A4}
$$

$$
\begin{aligned}
B_1 &= 2p(\tau_0 c_{44}^M \varepsilon_{11}^I + \left(\tau_0 c_{44}^M + E_0 c_{44}^M e_{15}^I\right) \varepsilon_{11}^M + \tau_0 c_{44}^M \varepsilon_{11}^S + E_0 c_{44}^M e_{15}^S \varepsilon_{11}^M \\
&+ \left(E_0 c_{44}^M \varepsilon_{11}^M + e_{15}^I \tau_0 + \tau_0 e_{15}^S + (E_0 e_{15}^S + E_0 e_{15}^I + \tau_0 + e_{15}^M E_0) e_{15}^M\right) e_{15}^M \\
&+ (-\tau_0 c_{44}^M \varepsilon_{11}^I + \left(-E_0 c_{44}^M e_{15}^I + \tau_0 c_{44}^M\right) \varepsilon_{11}^M + \tau_0 c_{44}^M \varepsilon_{11}^S + E_0 c_{44}^M e_{15}^S \varepsilon_{11}^M \\
&+ (-e_{15}^I \tau_0 + E_0 c_{44}^M \varepsilon_{11}^M + \tau_0 e_{15}^S + (-e_{15}^I E_0 + e_{15}^S E_0 + \tau_0 \\
&+ e_{15}^M E_0) e_{15}^M) e_{15}^M) q) / c_{44}^M / ((c_{44}^M - c_{44}^S + c_{44}^I) \varepsilon_{11}^I + (e_{15}^I)^2 \\
&+ (c_{44}^M - c_{44}^S + c_{44}^I) \varepsilon_{11}^M + (c_{44}^M - c_{44}^S + c_{44}^I) \varepsilon_{11}^S - (e_{15}^S)^2 + (2e_{15}^I + e_{15}^M) e_{15}^M \\
&+ (-2(e_{15}^I)^2 - 2c_{44}^I \varepsilon_{11}^I + (2c_{44}^M - 2c_{44}^S) \varepsilon_{11}^M + (2c_{44}^M - 2c_{44}^S) \varepsilon_{11}^S \\
&- 2(e_{15}^S)^2 + 2(e_{15}^M)^2 + ((-c_{44}^M + c_{44}^I + c_{44}^S) \varepsilon_{11}^I + (e_{15}^I)^2 \\
&+ (c_{44}^M - c_{44}^S - c_{44}^I) \varepsilon_{11}^M + (c_{44}^M - c_{44}^S - c_{44}^I) \varepsilon_{11}^S - (e_{15}^S)^2 \\
&+ (-2e_{15}^I + e_{15}^M) e_{15}^M) q) q)
\end{aligned} \tag{A5}
$$

$$
\begin{aligned}
B_2 &= 2pq(\tau_0 c_{44}^M \varepsilon_{11}^I + \left(\tau_0 c_{44}^M + E_0 c_{44}^M e_{15}^I\right) \varepsilon_{11}^M + \tau_0 c_{44}^M \varepsilon_{11}^S + E_0 c_{44}^M e_{15}^S \varepsilon_{11}^M \\
&+ \left(E_0 c_{44}^M \varepsilon_{11}^M + e_{15}^I \tau_0 + \tau_0 e_{15}^S + \left(E_0 e_{15}^S + E_0 e_{15}^I + \tau_0 + e_{15}^M E_0\right) e_{15}^M\right) e_{15}^M \\
&+ (-\tau_0 c_{44}^M \varepsilon_{11}^I + \left(-E_0 c_{44}^M e_{15}^I + \tau_0 c_{44}^M\right) \varepsilon_{11}^M + \tau_0 c_{44}^M \varepsilon_{11}^S + E_0 c_{44}^M e_{15}^S \varepsilon_{11}^M \\
&+ (-e_{15}^I \tau_0 + E_0 c_{44}^M \varepsilon_{11}^M + \tau_0 e_{15}^S \\
&+ \left(-E_0 e_{15}^I + E_0 e_{15}^S + \tau_0 + E_0 e_{15}^M\right) e_{15}^M) e_{15}^M) q) / c_{44}^M / ((c_{44}^M - c_{44}^S + c_{44}^I) \varepsilon_{11}^I \\
&+ (e_{15}^I)^2 + (c_{44}^M - c_{44}^S + c_{44}^I) \varepsilon_{11}^M + (c_{44}^M - c_{44}^S + c_{44}^I) \varepsilon_{11}^S - (e_{15}^S)^2 \\
&+ (2e_{15}^I + e_{15}^M) e_{15}^M + (-2(e_{15}^I)^2 - 2c_{44}^I \times \varepsilon_{11}^I + (2c_{44}^M - 2c_{44}^S) \varepsilon_{11}^M \\
&+ (2c_{44}^M - 2c_{44}^S) \varepsilon_{11}^S - 2(e_{15}^S)^2 + 2(e_{15}^M)^2 + ((-c_{44}^M + c_{44}^I + c_{44}^S) \varepsilon_{11}^I \\
&+ (e_{15}^I)^2 + (c_{44}^M - c_{44}^S - c_{44}^I) \varepsilon_{11}^M + (c_{44}^M - c_{44}^S - c_{44}^I) \varepsilon_{11}^S - (e_{15}^S)^2 \\
&+ (-2e_{15}^I + e_{15}^M) e_{15}^M) q) q)
\end{aligned} \tag{A6}
$$

$$
\begin{aligned}
B_3 &= -2p(-\tau_0 c_{44}^M e_{15}^I + \left(E_0 c_{44}^I - E_0 c_{44}^S + E_0 c_{44}^M\right) c_{44}^M \varepsilon_{11}^M \\
&+ \tau_0 c_{44}^M e_{15}^S + \left(\tau_0 c_{44}^I - \tau_0 c_{44}^S + \left(E_0 c_{44}^I - E_0 c_{44}^S + E_0 c_{44}^M\right) e_{15}^M\right) e_{15}^M \\
&+ (\tau_0 c_{44}^M e_{15}^I + (-E_0 c_{44}^I + E_0 c_{44}^M - E_0 c_{44}^S) c_{44}^M \varepsilon_{11}^M + \tau_0 c_{44}^M e_{15}^S \\
&+ (-\tau_0 c_{44}^S - \tau_0 c_{44}^I + (-E_0 c_{44}^I + E_0 c_{44}^M - E_0 c_{44}^S) e_{15}^M) e_{15}^M) q) \\
&/ c_{44}^M / ((c_{44}^M - c_{44}^S + c_{44}^I) \varepsilon_{11}^I + (e_{15}^I)^2 + (c_{44}^M - c_{44}^S + c_{44}^I) \varepsilon_{11}^M \\
&+ (c_{44}^M - c_{44}^S + c_{44}^I) \varepsilon_{11}^S - (e_{15}^S)^2 + (2e_{15}^I + e_{15}^M) e_{15}^M + (-2(e_{15}^I)^2 \\
&- 2c_{44}^I \varepsilon_{11}^I + (2c_{44}^M - 2c_{44}^S) \varepsilon_{11}^M + (2c_{44}^M - 2c_{44}^S) \varepsilon_{11}^S - 2(e_{15}^S)^2 \\
&+ 2(e_{15}^M)^2 + ((-c_{44}^M + c_{44}^I + c_{44}^S) \varepsilon_{11}^I + (e_{15}^I)^2 + (c_{44}^M - c_{44}^S - c_{44}^I) \varepsilon_{11}^M \\
&+ (c_{44}^M - c_{44}^S - c_{44}^I) \varepsilon_{11}^S - (e_{15}^S)^2 + (-2e_{15}^I + e_{15}^M) e_{15}^M) q) q)
\end{aligned} \tag{A7}
$$

$$
\begin{aligned}
B_4 = &-2pq(-\tau_0 c_{44}^M e_{15}^I + \left(E_0 c_{44}^I - E_0 c_{44}^S + E_0 c_{44}^M\right) c_{44}^M \varepsilon_{11}^M \\
&+\tau_0 c_{44}^M e_{15}^S + (\tau_0 c_{44}^I - \tau_0 c_{44}^S + (E_0 c_{44}^I - E_0 c_{44}^S + E_0 c_{44}^M) e_{15}^M) e_{15}^M \\
&+(\tau_0 c_{44}^M e_{15}^I + \left(-E_0 c_{44}^I + E_0 c_{44}^M - E_0 c_{44}^S\right) c_{44}^M \varepsilon_{11}^M + \tau_0 c_{44}^M \\
&\times e_{15}^S + (-\tau_0 c_{44}^S - \tau_0 c_{44}^I + (-E_0 c_{44}^i + E_0 c_{44}^M \\
&-E_0 c_{44}^S) e_{15}^M) e_{15}^M) q)/c_{44}^M/((c_{44}^M - c_{44}^S + c_{44}^I) \times \varepsilon_{11}^I + (e_{15}^I)^2 \\
&+(c_{44}^M - c_{44}^S + c_{44}^I)\varepsilon_{11}^M + (c_{44}^M - c_{44}^S + c_{44}^I)\varepsilon_{11}^S - (e_{15}^S)^2 \\
&+(2e_{15}^I + e_{15}^M) e_{15}^M + (-2(e_{15}^I)^2 - 2c_{44}^I \varepsilon_{11}^I + (2c_{44}^M - 2c_{44}^S)\varepsilon_{11}^M \\
&+(2c_{44}^M - 2c_{44}^S)\varepsilon_{11}^S - 2(e_{15}^S)^2 + 2(e_{15}^M)^2 + ((-c_{44}^M + c_{44}^I + c_{44}^S)\varepsilon_{11}^I \\
&+(e_{15}^I)^2 + (c_{44}^M - c_{44}^S - c_{44}^I)\varepsilon_{11}^M + (c_{44}^M - c_{44}^S - c_{44}^I)\varepsilon_{11}^S - (e_{15}^S)^2 \\
&+(-2e_{15}^I + e_{15}^M) e_{15}^M) q) q)
\end{aligned}
\tag{A8}
$$